High-Purity Nitrogen by Pressure-Swing Adsorption

Arthur I. Shirley and Norberto O. Lemcoff
The BOC Group, Murray Hill, NJ 07974

The separation of air for nitrogen production can be carried out by pressure-swing adsorption over a carbon molecular sieve. The separation is kinetically based, since the equilibrium adsorption of both oxygen and nitrogen is very similar, but the oxygen is adsorbed faster. Several theoretical and experimental studies have been reported, but mainly dealing with nitrogen purities below 99.9%. The objective of this article is to study experimentally the effect of different process variables on the performance of a rate-induced PSA process in the high-purity region. The effect of cycle time on both the yield and the specific product per unit cycle become more significant as the purity increases. On the other hand, the specific feed per unit cycle is almost insensitive to product purity, particularly as the cycle time increases. These results agree very well with predictions from a theoretical model.

Introduction

Pressure swing adsorption (PSA) has become a subject of interest in gas separations because of its low energy requirement and cost. The basic steps involved in a cycle are typically pressurization, high-pressure adsorption, equalization, countercurrent blowdown, and purge. PSA processes have found widespread application in hydrogen purification, air drying, and air separation (Yang, 1987). In the first two cases, the separation takes place because of the difference in the equilibrium adsorption isotherms of the components of the gas mixture. On the other hand, the separation of nitrogen from air on a carbon molecular sieve, is kinetically controlled. The adsorption equilibrium isotherms of oxygen and nitrogen are almost identical, and the preferential sorption of oxygen in these adsorbents results from the faster adsorption of that species on the carbon molecular sieve. Recently, several theoretical and experimental studies of a kinetically controlled PSA separation have been reported (Yang and Doong, 1985; Hassan et al., 1986, 1987; Shin and Knaebel, 1987, 1988; LaCava et al., 1989a,b; Farooq and Ruthven, 1990; Ruthven and Farooq, 1990; Lemcoff and LaCava, 1992; Lemcoff et al., 1993; Shirley and LaCava, 1993; Ng et al., 1993). Hassan et al. (1986, 1987) studied air separation on a carbon molecular sieve using different pressure-swing adsorption cycles. The linear driving-force model was found to adequately represent the experimental results. They also observed that the purity goes through a maximum as the cycle time increases, and that the yield increases with selectivity. Shin and Knaebel (1987, 1988) studied the separation of nitrogen from air using different molecular sieves, and compared the experimental measurements with the predictions of a pore-diffusion model. They examined the effect of several process variables on the performance, and found that there is a trade-off between purity and yield, which is characteristic of the diffusion-induced separations. Farooq and Ruthven (1990, 1991) and Ruthven and Farooq (1990) studied the separation of air using both a carbon molecular sieve and a modified zeolite. They observed a good agreement between experimental data with results from simulation studies using different models. The pore-diffusion model shows a closer agreement than the linear driving-force model, but it is computationally more time-consuming. They also found that the carbon molecular sieve gives a higher yield than the zeolite in the low-purity region. For oxygen concentrations lower than 1%, similar yield can be achieved with both sieves, but the zeolite has higher productivity. However, neither of the preceding studies have analyzed in detail the high-purity region, nor has a theoretical model been shown to adequately predict the performance in that region.

The objective of this article is to study the effect of different process variables, especially the cycle time, on the per-

Correspondence concerning this article should be addressed to N. O. Lemcoff.

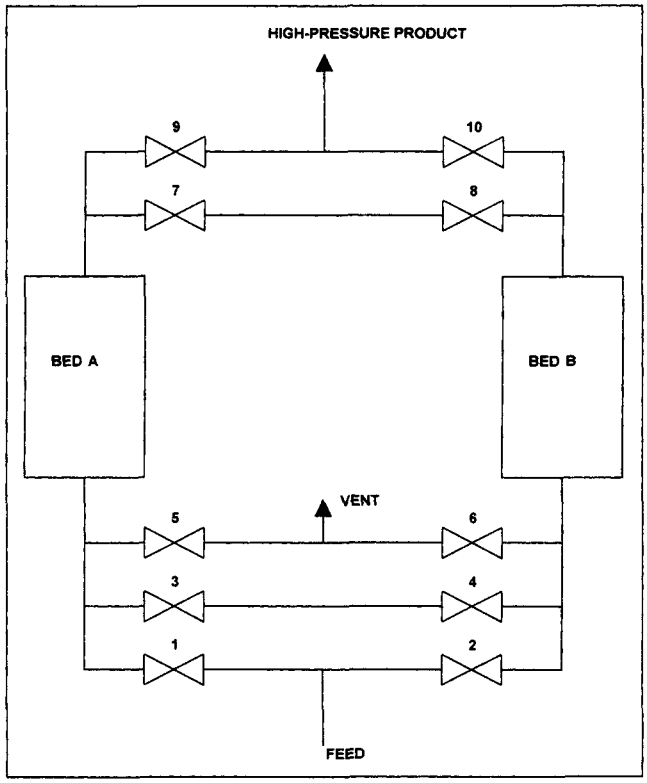

Figure 1. Pressure-swing adsorber.

Valve numbers refer to Figure 2 cycle sequence.

		FULL CYCLE SEQUENCE			
TIME (SEC) / VALVE POSITION		4	116-596	4	116-596
FEED TO BED A	1				
FEED TO BED B	2				
BOTTOM BALANCE	3				
BOTTOM BALANCE	4				
BED A VENT	5				
BED B VENT	6				
TOP BALANCE	7				
TOP BALANCE	8				
PRODUCT FROM BED A	9				
PRODUCT FROM BED B	10				

Figure 2. Valve sequencing for the PSA cycle.

■ Open; □ closed.

formance of a rate-induced PSA process in the high-purity region, and to compare the experimental results with the predictions of a theoretical model, thereby testing the ability of the model to cover both the high- and low-purity regions.

Experimental Studies

The experiments were carried in a commercial-scale two-bed nitrogen PSA unit built by The BOC Group, Inc. The adsorbent beds contained 1.2 m^3 of commercial carbon molecular sieve supplied by Generon Systems, Inc. The adsorbent was an extrudate with an average diameter of 2.5 mm and a bulk density of 630 kg/m^3. The PSA unit typically runs a series of four processing steps in cyclic fashion. In the first step of a cycle, one bed is pressurized with air while cocurrently producing nitrogen gas, while the second bed is regenerated by venting countercurrently to the atmosphere or to a vacuum. At the end of this first step both the product and feed ends of the beds are brought into fluid communication, causing gases from the bed at high pressure to flow into the regenerated bed until pressure equalization occurs. During regeneration the low-pressure bed is sometimes purged with a small fraction of the purified product stream, although this was not done in the experiments described this article. Pressurization of the adsorber beds was controlled according to the optimal method disclosed by Shirley and LaCava (1993). The repressurization process involves first slowly introducing feed gas for an initial period into the bed inlet to raise the bed pressure to an intermediate pressure less than the production pressure. Subsequently, the feed gas is rapidly introduced for a second period less than the initial period until the production pressure is reached. The PSA unit used in the experiments is shown in Figure 1. A full cycle on the PSA plant is shown in Table 1, while the typical timing and valve positions are represented in Figure 2.

Cycle times between 120 and 1,200 s, and specific products between 4.5 and 55 $Nm^3/m^3 \cdot h$ at 6.8×10^5 Pa adsorption pressure were tested. The measured gas flow rate is converted to Normal conditions (0°C and 1 atm).

Regeneration was done at atmospheric pressure in all cases. The change in the cycle time was achieved by changing simultaneously the duration of the production and venting steps. The duration of the remaining steps, pressurization, blowdown, and equalization, were not modified. To carry out the measurements at different purities, the product flow is varied by adjusting a valve, while all the other variables are maintained constant. After the steady state is reached, the flows and oxygen concentration are recorded, and a new adjustment of the valve is made.

Theoretical Model

Numerical simulations were carried out using the dynamic adsorption process simulator (DAPS), developed by LaCava et al. (1989a). The following assumptions were made in the development of the simulator:

Table 1. Cycle Description

Step	Adsorbent Bed A		Adsorbent Bed B
1	Pressurization		Regeneration
2	Continued feed and product release		Regeneration
3		Equalization	
4	Regeneration		Pressurization
5	Regeneration		Continued feed and product release
6		Equalization	

• The system is nonisothermal, but the thermal effects are very small, with the temperature fluctuating by less than 2°C.

• The total pressure remains constant during the production and purge steps. On the other hand, the pressure is assumed to increase linearly during pressurization, and follow an exponential decay during blowdown.

• The flow pattern is described by the axial dispersion model. The axial dispersion is variable point to point along the bed, a function of pressure and velocity.

• In the equalization step, the detailed composition profile for the pressurizing gas is taken from the corresponding profile of the depressurizing gas of the other bed (point-by-point model). During the regeneration step, there was no product purge.

• The rate of uptake of gases by non-Fickian carbon molecular sieves is described in terms of the slit-potential rate model (LaCava et al., 1989b), which considers the slit-cavity structure of the carbon molecular sieve. Under certain conditions, the Langmuir adsorption rate expression is a good approximation to the slit-potential-rate model, and it is used in the present work.

Model equations

Mass balance for component i in the fluid is given by

$$\epsilon\frac{\delta C_i}{\delta t} = D_A\frac{\delta^2 C_i}{\delta z^2} - \frac{\delta(v_z C_i)}{\delta z} - (1-\epsilon)R_i,$$

where the rate of adsorption is

$$R_i = \frac{\delta q_i}{\delta t} = k_{di}\, q_{mi}[K_i\, C_i(1-\Sigma\,\theta_k) - \theta_i].$$

The boundary conditions for the production step are

$$C_i(0,t) = C_{iF} + \frac{D_{iA}}{v_z}\frac{\delta C_i}{\delta z}\bigg|_{z=0}$$

$$\frac{\delta C_i}{\delta z}(L,t) = 0 \qquad v_z(L,t) = V_{\text{prod}}.$$

For the pressurization step, the only different boundary condition is the velocity at the top of the bed:

$$v_z(L,t) = 0.$$

During the vent step, the dispersion effect is neglected, and the boundary conditions are:

$$\frac{\delta C_i}{\delta z}(L,t) = 0 \qquad v_z(L,t) = 0.$$

Kinetic and equilibrium data were obtained using a batch-column device under conditions of constant temperature and volume. Pressure was measured continuously using a Datametrics pressure transducer and recorded with a Hewlett-Packard data-acquisition system (Koss et al., 1986; LaCava et al., 1989b). At 25°C the oxygen and nitrogen monolayer capacity is 1.8×10^{-3} kmol/kg CMS, and the adsorption and desorption kinetic constants are, respectively, 7.684×10^{-2} m^3/kmol s and 0.0176 L/s for oxygen, and 3.11×10^{-3} m^3/kmol s and 0.000585 L/s for nitrogen.

The PSA performance is determined in terms of the specific product and yield at a certain nitrogen product purity. The specific product is defined as the product flow rate per unit adsorbent volume, while the yield is the ratio between the net flow rate of nitrogen produced and the flow rate of nitrogen fed to the system. The specific feed, in turn, is defined as the feed flow rate per unit of adsorbent volume. In order to make comparisons between the experimental and computational results the data were normalized according to their values at a given reference point: 1% oxygen product concentration at 360-s cycle time. In addition, the specific feed and specific product data were placed on a per-cycle basis (rather than a per-unit time basis) so as to separate the data on the graphs, for ease of reading. Accordingly, the data are shown graphically as either product/cycle, feed/cycle, or the ratio product/feed, which is a measurement of the yield.

Results and Discussion

The experimental results obtained are shown graphically in Figures 3a through 5a. Figure 3a is a plot of the product per cycle vs. the product purity, while Figure 4a is a plot of the product yield (product/feed ratio) vs. the product purity.

In the low-purity regime, where the range of product purity varies from 0.1% to 10.0% O_2 (1,000 to 100,000 ppm O_2), both the product per cycle and yield tend to converge, indicating that the purification of product is relatively inde-

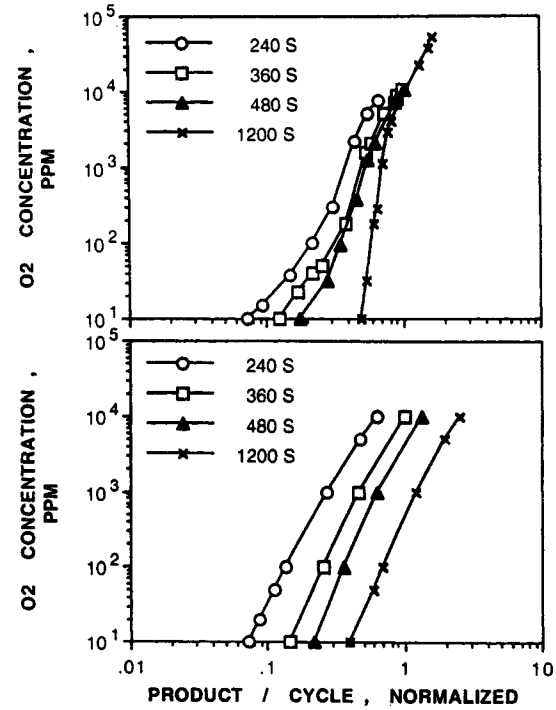

Figure 3. Product rate (product flow/cycle, normalized) as a function of product purity (ppm O_2) for four cycle times.

Top: experimental; bottom: predicted.

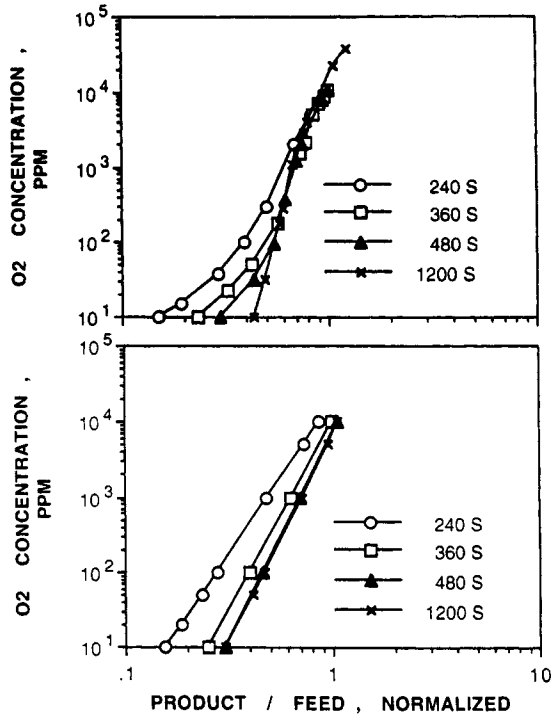

Figure 4. Product yield (product flow/feed flow, normalized) as a function of product purity (ppm O_2) for four cycle times.

Top: experimental; bottom: predicted.

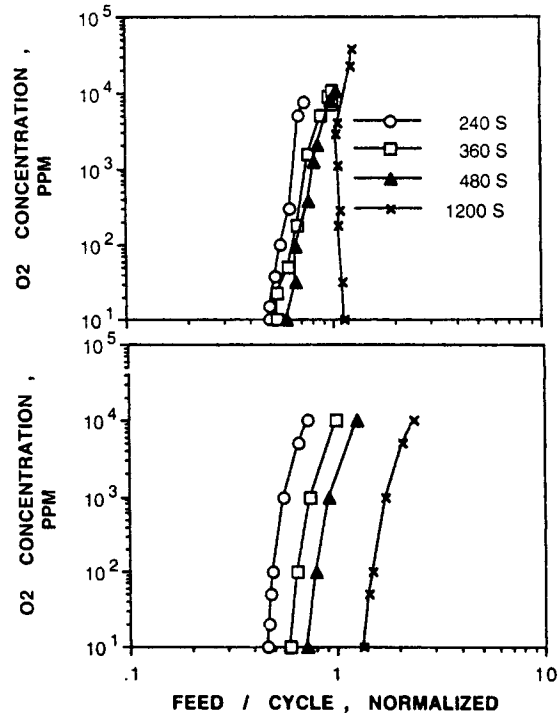

Figure 5. Feed rate (feed flow/cycle, normalized) as a function of product purity (ppm O_2) for four cycle times.

Top: experimental; bottom: predicted.

pendent of cycle time. This could only be so if the shape of the mass-transfer zone (MTZ) is insensitive to the cycle time at low purities (Schork et al., 1993). It would be expected that the MTZ would span the length of the adsorbent bed in the low-purity region, because of the small amount of O_2 adsorbed (Ng et al., 1993). In addition, in this region the throughputs are high (specific product/cycle/pore volume $\gg 1$), meaning that the average exposure time of a molecule to the CMS is small relative to the cycle time. This would also cause the shape of the MTZ to tend toward being cycle time-independent.

In the high-purity region, that is, product purities from 0.001% to 0.1% O_2 (10 to 1,000 ppm O_2), the curves in Figures 3a and 4a have a greatly different behavior. The product/cycle curves begin to diverge in greater degree as the product becomes more pure, while the product yield curves begin to separate one-by-one as the purity goes up. The shortest cycle times give the lowest amount of product per cycle as well as the lowest yields. The longest cycle time, 1,200 s, has the smallest variation in product/cycle as the purity goes up, while the shortest cycle time, 240 s, has the greatest variation. It is also interesting to note the "breakpoints" at which individual yield curves separate from others: about 5,000 ppm O_2 for a 240-s cycle time; about 170 ppm for 360-s; and about 100 ppm for 480 s. Although the mechanistic cause for this behavior is unknown, it is most probably related to the diffusional limitations of the adsorbent to purify a portion of the feed within the allotted cycle time. As the purity requirement increases more oxygen needs to be adsorbed, requiring a longer exposure time for that uptake to occur.

While the product/cycle and product/feed ratios show distinctly similar behavior in both the high- and low-purity regions, a plot of the specific feed multiplied by the cycle time vs. the product purity differs from these parameters altogether. Figure 5a is a plot of the specific feed multiplied by the cycle time vs. the product purity. The feed/cycle ratio is a measure of the amount of air processed per cycle to achieve a certain purity. As can be seen from Figure 5a, the feed/cycle values are fairly insensitive to product purity, particularly as the cycle time increases. This insensitivity of the feed/cycle to purity is even greater when one considers that a portion of the feed ends up as product, and that the volume of product decreases as the purity increases. If only the amount that is vented from the adsorbers as waste is considered (feed−product), this parameter is almost independent of purity.

The results from the simulation studies at 6.8×10^5 Pa (85 psig) adsorption pressure and different cycle times are represented in Figures 3b–5b. A direct comparison between the predicted values and the experimental measurements at two cycle times is shown in Figures 6–8. A good agreement is observed, specially at high purities. The dependence of both product/cycle and product/feed on the oxygen concentration increases as the cycle time decreases. It can be seen that at 1% (10,000 ppm) oxygen in the product, the product/cycle at 240-s cycle time is less than the value at 1,200-s cycle time, as it is at an oxygen concentration of 10 ppm. The yield measured at 240-s cycle time, in the range of oxygen concentrations considered, is always lower than that at 1,200 s. However, the difference is smaller at the higher oxygen concentration.

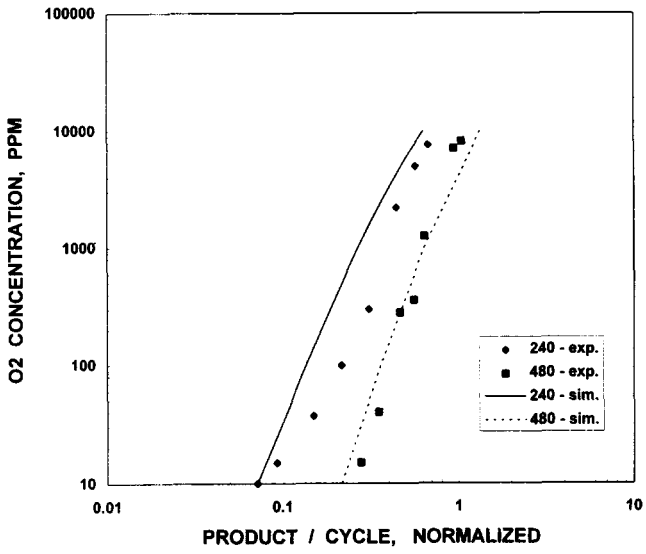

Figure 6. Comparison between the predicted and experimental product rate for two cycle times.

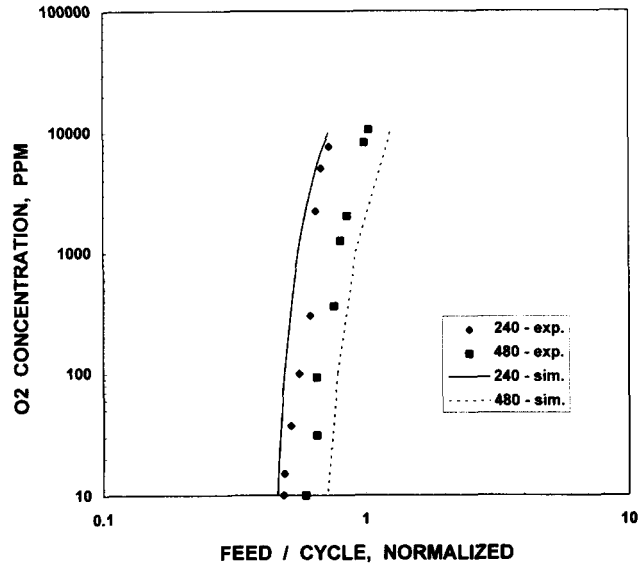

Figure 8. Comparison between the predicted and experimental feed rate for two cycle times.

The product/cycle data shown in Figures 3a and 3b represent the amount of nitrogen produced per unit bed volume during the cycle. It can be seen that this amount increases with cycle time, and also as the purity decreases. Due to the kinetic control of the adsorption of nitrogen from air, as the cycle time increases more gas is adsorbed during the adsorption step. Since oxygen adsorbs faster than nitrogen, higher purities can be achieved for the same nitrogen production rate, or at a constant purity, higher production rates can be reached. In the high-purity regime there is good agreement between the calculated and experimental data. The largest disagreement appears to occur for the product/cycle data at 1,200-s cycle time in the low-purity regime, where the calculated values are much greater than the experimental values.

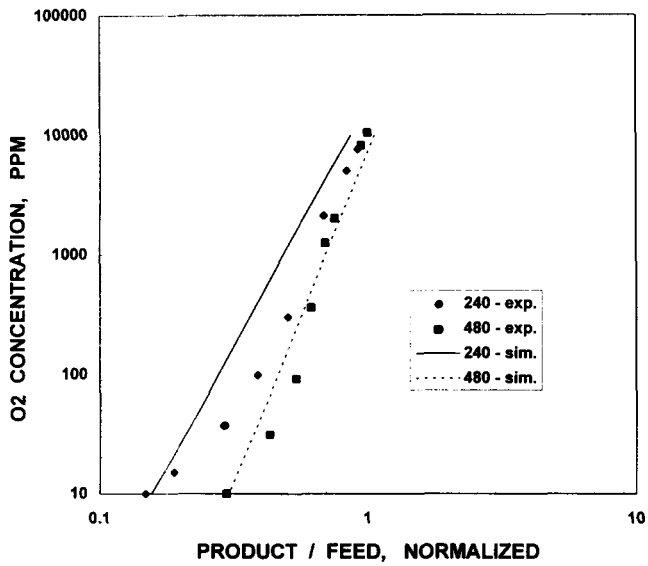

Figure 7. Comparison between the predicted and experimental product yield for two cycle times.

This can be attributed to the different pressurization rate, which has been shown to affect the process performance (Shirley and LaCava, 1993).

A reasonable agreement between the experimental and calculated values of the product/feed ratio is shown in Figure 7. While both sets of data tend to converge in the low-purity regime, there is more curvature to the experimental curves than the calculated curves, although the significance of this is not understood.

The calculated values of feed/cycle as a function of product concentration also compare well with the experimental data (Figure 8). Here the simulator overpredicts the amount of feed air necessary to produce product at a given purity by about 20% in the high-purity region. This overprediction may be due to faster kinetics assumed in the simulator than actually exists in CMS.

Of course, as Figures 3 and 4 show, both the product/cycle and product/feed tend to zero as the product purity goes to 0 ppm, but the feed/cycle (Figure 5) goes to some finite, limiting value. By extrapolating the experimental and calculated data to product/cycle values of zero, the limiting values of the feed/cycle can be determined. These values reflect the amount of air needed to bring the adsorber vessels up to the production pressure, including the amount needed for adsorption as well as that needed to fill the interstitial and pore volumes in the CMS. In short, they represent on a bulk scale what microbalance experiments represent on a small scale: the effect of exposure time on uptake. When plotted against the part (half) cycle time (Figure 9), the limiting feed/cycle is a gross measure of the adsorption kinetics of air. At short cycle times the majority of the limiting feed is due to the gas needed to fill the interstitial space in the adsorbent beds, such that very little nitrogen purification occurs, while at long cycle times the adsorption of both nitrogen and oxygen is near equilibrium levels with little nitrogen purification, again. Interpolation of the data gives an adsorption half-time of about 1,600 s, which matches closely that for air at the same pressures from batch adsorption experiments.

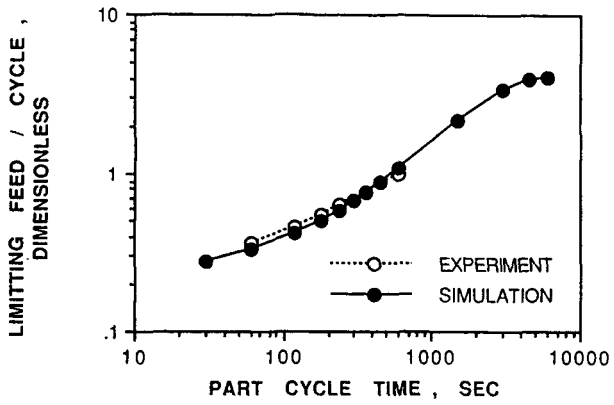

Figure 9. Computed and experimental limiting feed rate (feed flow/cycle, normalized) as a function of part cycle time.

Conclusions

The separation of air by pressure swing adsorption on a carbon molecular sieve has been studied both experimentally and numerically over a wide range of product purities. A good agreement has been found between the experimental results and the predictions of dynamic adsorption process simulator (DAPS) over a wide range of purities.

In the low-purity region both the specific product and yield tend to converge, and the product purity is independent of cycle time, while in the high-purity region the performance improves as the cycle time increases. A greater effect of the oxygen concentration of the product on the performance is observed at the shorter cycles.

The limiting values of feed/cycle were used to estimate the adsorption half-time for air in the adsorber vessels. The value matched closely that obtained from batch adsorption experiments.

Notation

C = gas-phase concentration, kmol/m^3
D_A = axial dispersion coefficient, m^2/s
K = Langmuir equilibrium constant, m^3/kmol
k_d = Langmuir desorption constant, L/s
L = bed length, m
q = adsorbed phase concentration, kmol/m^3
q_m = monolayer capacity, kmol/m^3
t = time, s
V_{prod} = gas exit velocity during production step, m/s
v_z = axial gas velocity, m/s
z = axial distance, m
ϵ = bed voidage
$\theta = q/q_m$

Subscripts

F = feed value
k = component k

Literature Cited

Farooq, S., and D. M. Ruthven, "A Comparison of Linear Driving Force and Pore Diffusion Models for a Pressure Swing Adsorption Bulk Separation Process," *Chem. Eng. Sci.*, **45**, 107 (1990).

Farooq, S., and D. M. Ruthven, "Numerical Simulation of a Kinetically Controlled Pressure Swing Adsorption Bulk Separation Process Based on a Diffusion Model," *Chem. Eng. Sci.*, **46**, 2213 (1991).

Hassan, M. M., N. S. Raghavan, and D. M. Ruthven, "Air Separation by Pressure Swing Adsorption on a Carbon Molecular Sieve," *Chem. Eng. Sci.*, **41**, 1331 (1986).

Hassan, M. M., N. S. Raghavan, and D. M. Ruthven, "Pressure Swing Adsorption Air Separation on a Carbon Molecular Sieve," *Chem. Eng. Sci.*, **42**, 2037 (1987).

Koss, V. A., D. A. Wickens, P. Cucka, and A. I. LaCava, "A Model of the Adsorption of Gases on Carbon Molecular Sieves with Langmuir's Kinetics and Simultaneous Diffusion," *Proc. Carbon 86*, Baden-Baden, Germany, p. 388 (1986).

LaCava, A., J. A. Dominguez, and J. Cardenas, *Adsorption: Science and Technology*, A. E. Rodrigues, M. D. LeVan, and D. Tondeur, eds., *NATO ASI Ser.*, **158**, p. 323 (1989a).

LaCava, A., V. A. Koss, and D. A. Wickens, "Non-fickian Adsorption Rate Behaviour of some Carbon Molecular Sieves," *Gas Sep. Purif.*, **3**, 180 (1989b).

Lemcoff, N. O., and A. I. LaCava, "Effect of Regeneration Pressure Level in Kinetically Controlled Pressure Swing Adsorption," *Gas Sep. Purif.*, **6**, 9 (1992).

Lemcoff, N. O., S. J. Doong, and A. I. LaCava, "Modeling of Equalization in Air Separation by Pressure Swing Adsorption," *Proc. Int. Conf. on the Fundamentals of Adsorption*, M. Suzuki, ed., Kodansha, Tokyo, p. 357 (1993).

Ng, M., J. M. Schork, and K. R. Fabregas, "The Mass Transfer Zone in Nitrogen PSA Columns," *Gas Sep. Purif.*, **7**, 159 (1993).

Ruthven, D. M., and S. Farooq, "Air Separation by Pressure Swing Adsorption," *Gas Sep. Purif.*, **4**, 141 (1990).

Schork, J. M., R. Srinivasan, and S. R. Auvil, "A Shortcut Computational Method for Designing N2 PSA Adsorbents," *Ind. Eng. Chem. Res.*, **32**, 2226 (1993).

Shin, H. S., and K. S. Knaebel, "Pressure Swing Adsorption: A Theoretical Study of Diffusion-Induced Separations," *AIChE J.*, **33**, 654 (1987).

Shin, H. S., and K. S. Knaebel, "Pressure Swing Adsorption: An Experimental Study of Diffusion-Induced Separation," *AIChE J.*, **34**, 1409 (1988).

Shirley, A. I., and A. I. LaCava, "Novel Pressurization Methods in Pressure Swing Adsorption Systems for the Generation of High Purity Gas," *Ind. Eng. Chem. Res.*, **32**, 906 (1993).

Yang, R. T., *Gas Separation by Adsorption Processes*, Butterworths, Boston (1987).

Yang, R. T., and S. J. Doong, "Gas Separation by Pressure Swing Adsorption: A Pore-Diffusion Model for Bulk Separation," *AIChE J.*, **31**, 1829 (1985).

Manuscript received Apr. 4, 1996, and revision received Aug. 26, 1996.